Temperature Dependence of Behavior of Interface between Molten Sn and LiCl–KCl Eutectic Melt Due to Rising Gas Bubble

Shungo Natsui*, Ryota Nashimoto, Hifumi Takai, Takehiko Kumagai,
Tatsuya Kikuchi, and Ryosuke O. Suzuki

Division of Materials Science and Engineering, Faculty of Engineering,
Hokkaido University,
Kita 13 Nishi 8, Kita–ku, Sapporo 060–8628, Japan.

*Corresponding author. Tel.: +81–11–706–6342
E–mail address: natsui@eng.hokudai.ac.jp

Keywords: molten metal–slag interface; bubbly flow; metal film; surface tension

Abstract:

The behavior of the interface between molten Sn and the LiCl–KCl eutectic melt system was observed directly. We found that the transient behavior of the interface exhibits considerable temperature dependence through a change in its physical properties. The "metal film" generated in the upper molten-salt phase significantly influences the shape of the interface. Although the lifetime of the metal film depends on the gas flow rate, it is not affected by the buoyancy if the interfacial tension is dominant.

Most extractive metallurgical treatments produce a two-liquid-phase system consisting of a metal-rich phase and a less-dense slag phase. The main purpose of such processes is to concentrate the metal phase into a form suitable for further refining and to efficiently remove the gangue materials as a molten slag. Gaseous phases, which are introduced into the liquid metal phase or produced there by reactions, pass through the metal–slag interface. As this happens, the rising gas bubbles might entrain the heavier liquid metal from the bottom layer into the top layer of the lighter molten slag. This will be either desirable or detrimental, depending on the application in question. In steelmaking, the entrainment of iron droplets in the slag can significantly increase mass transfer between the two immiscible liquids and thus greatly enhance the rate of the desired chemical reactions such as decarburization, desulphurization, and dephosphorization [1]. On the other hand, in copper smelting, the dispersed droplets of the copper-bearing matte are entrapped in the slag and can also cause financial losses, if the slag containing the copper droplets is discarded without further treatment [2].

Therefore, metal entrainment in the slag phase is of considerable practical interest. To quantitatively describe the chemical reactions occurring via the metal droplets in slag [3–5], the mechanism of droplet formation should be elucidated. Although several investigations in room-temperature media have been performed [6–11], data from direct observations in high-temperature systems are still rare, owing to the difficulties encountered in doing so. Chevrier and Cramb [12] observed bubble separation at the iron–slag interface using X-ray fluoroscopy techniques and confirmed the emulsification of metal droplets in the slag. Moreover, the phenomenon of bubble bursting in the gas–slag–iron system was investigated using the X-ray transmission technique [13–17]. These studies found two mechanisms for droplet formation, namely, jet entrainment and film entrainment. Nevertheless, in-situ X-ray observations of the dynamic behavior of the molten metal–slag interface have also proven difficult, owing to the extremely limited observation domain. That is to say, the behavior of a three-dimensional bubble cannot be clarified from a two-dimensional image analysis.

To understand the dynamic behavior of a liquid–liquid–gas interface, direct optical observations of the interfacial flow in a wide domain are necessary. However, the physical properties of the water ($\rho = 997$ kg/m^3, $\sigma = 7.2 \times 10^{-2}$ N/m) and oil ($\rho = 935$ kg/m^3, $\sigma = 2.0 \times 10^{-2}$ N/m) phases are too different to allow for a comparison with Fe ($\rho \cong 7000$ kg/m^3, $\sigma \cong 1.0$ N/m) and slag ($\rho \cong 3000$ kg/m^3, $\sigma \cong 0.4$ N/m) systems, as the "thin film" shape of a metal depends strongly on the physical properties of the metal and slag phases. The two immiscible melts of a low-melting-point metal and molten-salt system are particularly interesting. A molten

salt is clear and chemically stable, and it is possible to design the values of its physical properties. In an early study, Poggi et al. [18] investigated entrainment mechanisms using Pb/molten salt systems. Song et al. [19, 20] proposed an additional rupture phenomenon, wherein an elongated metal column is formed by two or three bubbles passing through the interface of an Al–Cu alloy/molten salt system. Here, a metal dome is first formed at the interface because of a rising gas bubble, with the successive bubbles reaching this interface before the initial bubble becomes detached, causing the metal column to extend further into the slag phase.

However, the behaviors of interfaces are difficult to study, even when they are formed between similar materials. The splitting of a single bubble occurs, owing to the slight difference in the conditions corresponding to high interfacial tension. The aim of this study was to elucidate the mechanisms of interfacial flow on the basis of three-dimensional shape observations. A LiCl–KCl eutectic melt (LiCl/KCl = 59:41 mol%, m.p. = 625 K(352 °C), which is widely used for electrolysis, was employed as the "slag phase." Molten Sn was used as the “metal phase” because its density is close to that of liquid Fe and Cu. The advantage of this system is that thermodynamic data on it is widely available and it exhibits thermal stability over a wide temperature range 650–900 K (377–627 °C). To simulate the various interfacial flow modes, we focused on the temperature dependence of the physical properties. This was done to clarify the sensitivity of the interfacial flow to changes in the physical properties (especially density and surface tension; the changes in the viscosity can be ignored, as discussed later). **Figure 1** shows a schematic diagram of the experimental apparatus used. A borosilicate glass crucible 100 mm in diameter and 250 mm in height was employed. It had a barrel-vaulted shape with a flat surface for in-situ observations. The gas injection nozzle was also made of borosilicate glass; its outer diameter and thickness were 8.0 and 1.5 mm, respectively. Sn shot (1,500 g) with a purity of 99.9 mass% was placed in the crucible. Approximately 520 g of the eutectic salts (LiCl: >99 mass%, KCl: >99.5 mass%, Wako Chemical Co.) were mixed and placed on the Sn shot. The electric resistance furnace was designed to allow the phenomena occurring within to be observed directly. The interface temperature was measured with a K–type thermocouple with a glass protection tube. The salt was dehydrated in vacuum at a temperature of 573 K(300 °C) or lower. After being dehydrated overnight, it was continuously heated to the desired melt temperature in an Ar gas atmosphere. Once the materials had melted completely, Ar (>99.999%) gas was blown through the glass pipe into the molten Sn at a desired gas flow rate using a mass flow controller (MQV9500, Azbil). The changes induced in the interface were recorded at a rate of 500–1000

frames per second and a resolution of 1024 × 1024 pixels using a high-speed video camera (Fastcam SA3, Photron Co., Ltd.). For each image captured, the location of the tip of the liquid–liquid interface was tracked using an image processing software (PFV Viewer, ver. 338).

First, we discuss the shapes of the interfaces formed because of a single rising bubble. **Figure 2** shows the behavior of the interface between the molten Sn and the LiCl–KCl eutectic melt as a single Ar gas bubble rose. The interface temperature was determined from the values displayed on the digital multimeter. At 856 K(583 °C) (Case 1), a single bubble reached the Sn–salt interface at t = 0.06 s. Then, a "metal dome" appeared. That is to say, the rising bubble started to modify the shape of the interface by pulling the Sn phase upward through the interface. At t = 0.12 s, this dome was ruptured, and the gas bubble started to penetrate the upper salt phase. Once it had fully penetrated the salt phase, the bubble rose up through the phase. The liquid–liquid interface was unsteady even after t = 0.30 s. At lower temperatures, the bubble behaviors were very different from those in Case 1. In Case 2, a single bubble reached the Sn–salt interface (t = 0.12 s) and started to disperse, penetrating the upper phase. The reason for this could be that, because of the lack of a buoyancy force, the gas bubble could not break through the Sn–salt interface after only one impact. At t = 0.18 s, the dome held the bubbles on the metal phase. It then ruptured at t = 0.24 s, after which the bubbles penetrated the slag phase. The process for Case 2 can be summarized as follows: first, a bubble was lifted by buoyancy. It sprung back, owing to the interfacial tension, after striking the interface once. The dome broke subsequently. On the other hand, in Case 3, the bubble did not penetrate the slag phase even after t = 0.30 s. We performed a number of experiments to confirm this phenomenon. The dependence of the detention time of the bubble in the Sn phase on the temperature is shown in **Fig. 3**. The behavior described above as Case 1 appeared only for T > 825 K (552 °C). For T < 825 K (552 °C), only Cases 2 and 3 were observed at every temperature. However, the detention time was longer, in particular, for 710 K(437 °C) < T < 790 K(517 °C). For 700 K(427 °C) < T < 800 K(527 °C), the fluctuation range was relatively large. The stability of the Sn film would be attributed primarily to these fluctuations in the bubble detention time. Based on Grace's diagram [27], a rising single bubble in molten Sn is assumed to be in the "wobbling" state. Owing to the instability of the metal–salt interface, the frequency of the interfacial fluctuations does not remain constant. Therefore, the error bar for the detention time must be extended for the conditions where the interfacial tension is dominant.

The shape of the interface formed between two materials varies greatly with

the physical properties of the materials, which can be expressed as a function of nondimensional parameters such as the Eötvös number ($= g\Delta\rho {d_b}^2/\sigma$), the Morton number ($= g\Delta\rho\mu^4/\rho^2\sigma^3$), and the Reynolds number ($= d_b\Delta\rho U/\mu$). These parameters indicate that a slight change in the physical properties (i.e., the density, ρ, viscosity, μ, surface tension, σ, and bubble diameter, d_b) would affect the interfacial flow significantly, even in systems with similar materials. We found that this tendency as seen in Fig. 3 corresponded well with the surface tension curve for Sn given by Yuan et al. [21]. The physical properties of molten Sn and the LiCl–KCl eutectic melt are listed in **Table 1** [21–24]. Thus, the focus should be on the dynamic balance between the surface tension and the buoyancy force, if one wishes to clarify the dome formation mechanism. Here, the size of a single bubble, d_b, is predicted from the equation for d_b, which is derived while assuming that bubble formation occurs at the tip of a nozzle at a low flow rate such that only the outer diameter, d_o, is considered [12].

$$d_b = 3\sqrt{\frac{6d_o\sigma}{\rho \mathrm{g}}} \tag{1}$$

where ρ and σ are the density and surface tension of the metal, respectively. From this equation, the bubble diameter, d_b, in molten Sn was estimated to 6.356 mm at 850 K (577 °C) and 6.350 mm at 683 K (410 °C). The bubble diameter was probably not strongly affected over the range of temperatures investigated in this study. We investigated the effects of the viscosity using computational fluid dynamics simulations and found that the detention time of the bubble was not sensitive to changes in the viscosity [25, 28]. Thus, as stated above, the dynamic balance between the surface tension and the buoyancy force is critical for elucidating the dome formation mechanism. Nevertheless, the change in the surface tension was large in relation to the change in density. Consequently, we focused on the effects of the surface tension to clarify the conditions for "thin Sn film" formation.

The bubble detention time can be explained on the basis of a decrease in the Sn film thickness because of drainage. A simplified schematic diagram of the Sn–salt–Ar system is shown in **Fig. 4**. The thickness of the Sn film, e, decreases by pouring Sn into the lower part. For simplicity, we assumed that this "Sn bubble" was completely spherical with a constant radius R and that the film thickness, e, remained constant. By using the law describing the pressure difference between two dissimilar fluids (Laplace's pressure, $2\sigma/R$), the dynamic balance along the vertical direction of the film surface can be written as [26]

$$\frac{4\sigma}{R} - \rho g e \cos\theta = p_i - p_e \quad (2)$$

where p_i is the internal pressure in the film, and p_e is the external pressure. Because the second term on the left-hand side is sufficiently small, the internal pressure, p_i, is higher than p_e. In fact, the curvature radius, R, has a weak height dependence (through the angle θ in polar coordinates). Thus, the curvature is the smallest at the top of the Sn film. **Figure 5** shows snapshots of the gas–liquid interface obtained through in–situ observations performed at various times. Although the snapshots are two-dimensional, they show that a spherical bubble covered in a thin film of molten Sn rose in the molten salt, ruptured at 0.002 s, became detached at 0.004 s, and burst at the salt surface at 0.008 s. After the bubble had burst, the thin film of molten Sn became a spherical droplet. From these snapshots, the average thickness of the Sn film was estimated to be $\approx 50\,\mu m$. However, this could represent the ideal condition. The thickness, e, may actually be different at each location. Further, there probably exist heavier and lighter parts. This thickness gradient would cause a turbulent interfacial flow, resulting in the formation of an unstable phase boundary [26]. In this situation, the effect of the viscosity should also be considered if the drainage rate changes significantly.

Song et al. [19] stated that the gas flow rate is an important factor affecting the interface shape. Here, our interest was in the temperature dependence of the interface behavior for a large flow rate. The behavior of the interface between molten Sn and the LiCl–KCl eutectic melt during the ascent of Ar gas bubbles was observed. Representative photographs obtained at different temperatures are shown in **Fig. 6**. At 723 K (450 °C), an Ar gas bubble rose and reached the surface of the molten salt, during which process the bubble was completely covered with molten Sn. Thus, the molten Sn reached the molten salt's free surface. However, at 903 K (630 °C), the molten Sn did not reach the free surface because the formed thin Sn film ruptured while it was rising. In this case, the total buoyancy force was large because of the high flow rate, in contrast to the case for a single bubble, and the arrival height of the molten Sn increased as a result. The flow-rate dependence of the percentage of Sn film formation is shown in **Fig. 7**. Because the size of each bubble changed at a high flow rate, the interface shape was also affected by these fluctuations. It was assumed that film formation occurred when $\theta > \pi/2$. On one hand, the film formation ratio decreased with a decrease in the flow rate at 903 K (630 °C). A film was not formed by a single bubble; this was in keeping with Case 1 in Fig. 2. On the other hand, at 723 K (450 °C), the ratio of film formation was almost constant for all gas flow rates. From this result,

it was concluded that the lifetime of the film is not affected by the buoyancy when the interfacial tension is dominant.

This study was supported by the Japan Oil, Gas, and Metals National Corporation (JOGMEC).

References

1. D. Mazumdar, and R. I. L Guthrie: ISIJ Int., 1995, vol. 35, pp. 1–20.
2. G. Kaptay: Metall. Mater. Trans. B, 2001, vol. 32, pp. 555–557.
3. Subagyo and G. A. Brooks: ISIJ Int., 2002, vol. 42, pp. 1182–1184.
4. N. Dogan, G. A. Brooks, and M. A. Rhamdhani: ISIJ Int., 2011, vol. 51, pp. 1093–1101.
5. B. S. Terry, and P. Grieveson: ISIJ Int., 1993, vol. 33, pp. 166–175.
6. R. Minto, and W. G. Davenport: Can. Mining Metall. Bull., 1972, vol. 65, pp. 70–76.
7. G. Reiter, and K. Schwerdtfeger: ISIJ Int., 1992, vol. 32, pp. 50–56.
8. G. Reiter, and K. Schwerdtfeger: ISIJ Int., 1992, vol. 32, pp. 57–65.
9. Z. Lin, and R. I. L. Guthrie: Metall. Mater. Trans. B, 1994, vol. 25, pp. 855–864.
10. K. Sakaguchi, and K. Ito: ISIJ Int., 1995, vol. 35, pp. 1348–1353.
11. A. Kumar, M. Malathi, K. M. Godiwalla, E. Z. Chacko, S. K. Ajmani, and S. Ranganathan: ISIJ Int., 2014, vol. 54, pp. 2239–2247.
12. V. F. Chevrier, and A. W. Cramb: Metall. Mater. Trans. B, 2000, vol. 31, pp. 537–540.
13. M. Iguchi, T. Chihara, N. Takanashi, Y. Ogawa, N. Tokumitsu, and Z. I. Morita: ISIJ Int., 1995, vol. 35, pp. 1354–1361.
14. P. K. Iwamasa, and R. J. Fruehan: ISIJ Int., 1996, vol. 36, pp. 1319–1327.
15. Z. Han, and L. Holappa: Metall. Mater. Trans. B, 2003, vol. 34, pp. 525–532.
16. Z. Han, and L. Holappa: ISIJ Int., 2003, vol. 43, pp. 292–297.
17. L. Holappa, L. Forsbacka, and Z. Han: ISIJ Int., 2006, vol. 46, pp. 394–399.
18. D. Poggi, R. Minto, and G. Davenport: J. Met., 1969, vol. 21, pp. 40–45.

19. D. Y. Song, N. Maruoka, T. Maeyama, H. Shibata, and S. Y. Kitamura: ISIJ Int., 2010, vol. 50, pp. 1539–1545.
20. D. Y. Song, N. Maruoka, G. S. Gupta, H. Shibata, S. Y. Kitamura, and S. Kamble: Metall. Mater. Trans. B, 2012, vol. 43, pp. 973–983.
21. Z. Yuan, K. Mukai, K. Takagi, and M. Ohtaka: J. Japan Inst. Metals, 2001, vol. 65, pp. 21–28.
22. L. Wang and Q. Mei: J. Mater. Sci. Technol., 2006, vol. 22, pp. 569–571.
23. E. V. Rozhitsina, S. Gruner, I. Kaban, W. Hoyer, V. E. Sidorov, and P. S. Popel: Russ. Metall. (Metally), 2011, vol. 2011, pp. 118–121.
24. G. J. Janz, R. P. T. Tomkins, C. B. Allen, J. R. Downey Jr., G. L. Garner, U. Krebs, and S. K. Singer: J. Phys. Chem. Ref. Data, 1975, vol. 4, pp. 871–1178.
25. S. Natsui, H. Takai, T. Kumagai, T. Kikuchi, R. O. Suzuki: Mater. Trans., 2014, vol. 55, pp. 1707–1715.
26. P. de Gennes, F. Brochard–Wyart, and D. Quéré: Capillarity and Wetting Phenomena: Drops, Bubbles, Pearls, Waves, Yosioka Shoten, Kyoto, 2003, pp. 210–212.
27. J. R. Grace, Trans. Inst. Chem. Eng., 1973, vol. 51, pp. 116–120.
28. S. Natsui, R. Nashimoto, H. Takai, T. Kumagai, T. Kikuchi, and R. O. Suzuki, Chem. Eng. Sci., 2016, vol. 141, pp. 342–355.

Table and Figures

Table 1 Temperature–dependent equation for the physical properties of liquid Sn and the molten LiCl–KCl eutectic melt.

Fig. 1. Schematic diagram of the experimental setup used.

Fig. 2. Observed behavior of a single Ar gas bubble rising through the liquid Sn–molten salt interface at various temperatures. The flow rate of Ar gas was controlled at 0.067 ml/s to generate an isometric single bubble. Each snapshot shows the representative behavior in the corresponding temperature range.

Fig. 3. Temperature dependence of the detention time of a single Ar bubble in liquid Sn.

Fig. 4. Structure of a single Ar bubble covered by a liquid Sn film in the molten salt. Under this ideal condition, the film thickness, e, depends on θ.

Fig. 5. Snapshots of the interface of the liquid Sn film. The film ruptured starting at 0.002 s, and a single Ar gas bubble rose in the molten salt and burst at the salt surface. At 0.090 s, a metal drop became detached from the bubble. During this experiment, the system temperature was 823 K(550 °C), and the flow rate was 8.333 ml/s.

Fig. 6. Comparison of representative experimental photographs showing the behavior of the liquid Sn interface at each temperature. The flow rate of Ar gas was controlled at 8.333 ml/s.

Fig. 7. Gas flow rate dependence of the ratio of metal film formation at each temperature.

1

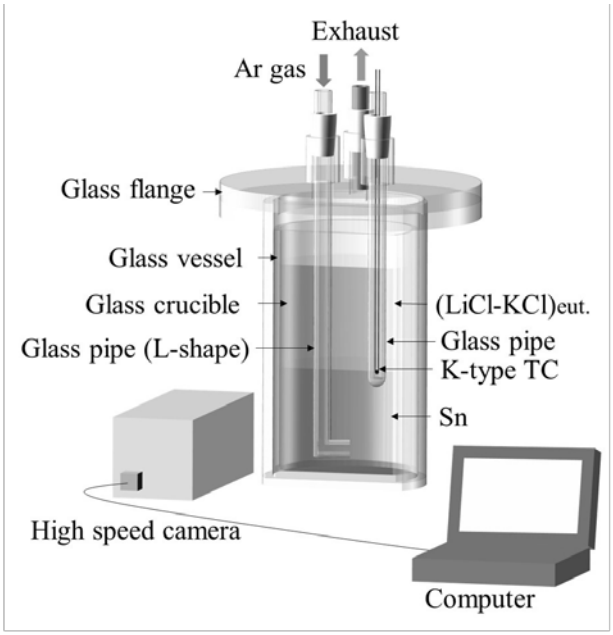

Fig. 1. Schematic diagram of experimental setup.

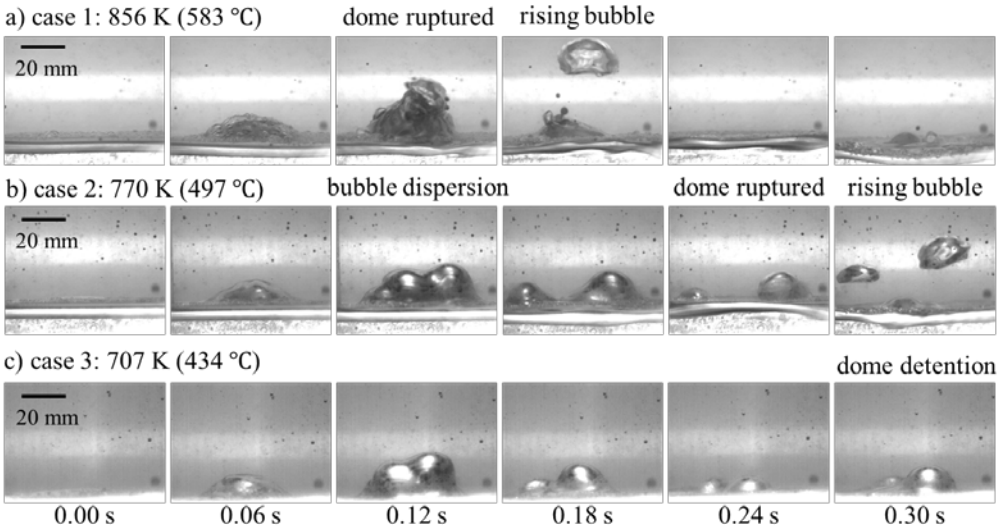

Fig. 2. Observed behavior of single Ar gas bubble rising through liquid Sn–molten salt interface at various temperatures. Flow rate of Ar gas is controlled at 0.067 ml/s to generate an isometric single bubble. Each snapshot shows representative behavior in their temperature range.

1

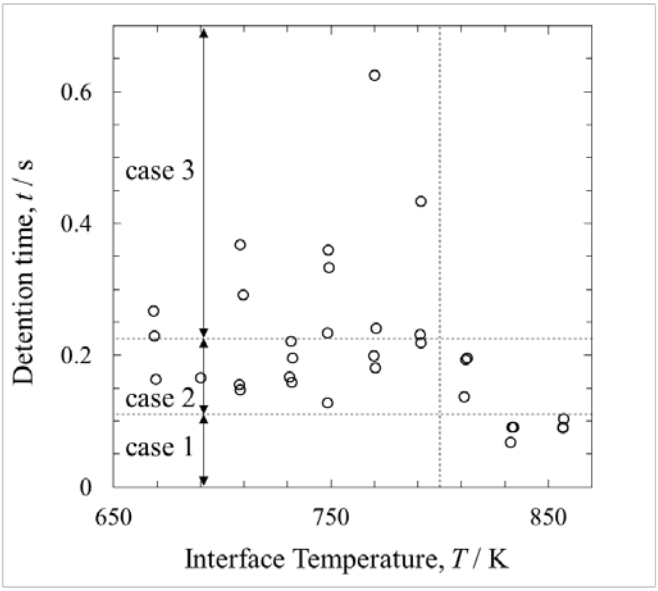

Fig. 3. Temperature dependence of detention time of single Ar bubble in liquid Sn.

1

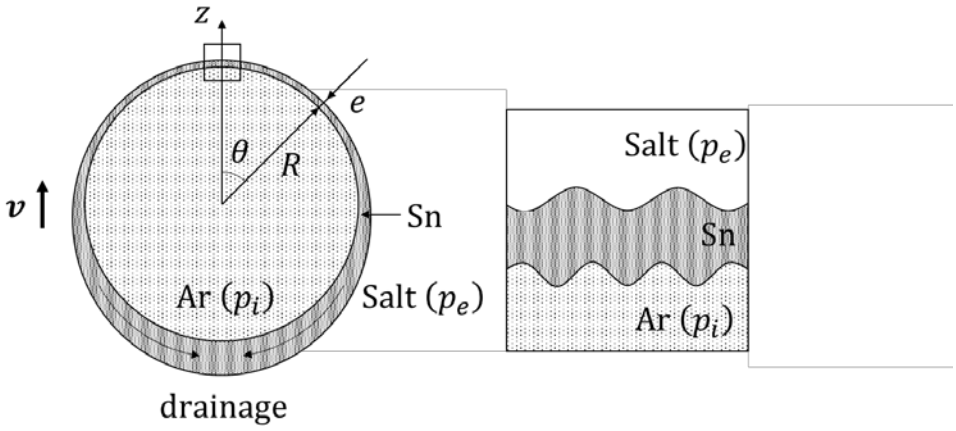

Fig. 4. Structure of single Ar bubble covered by a liquid Sn film in molten salt. In this ideal condition, the film thickness e depends on θ.

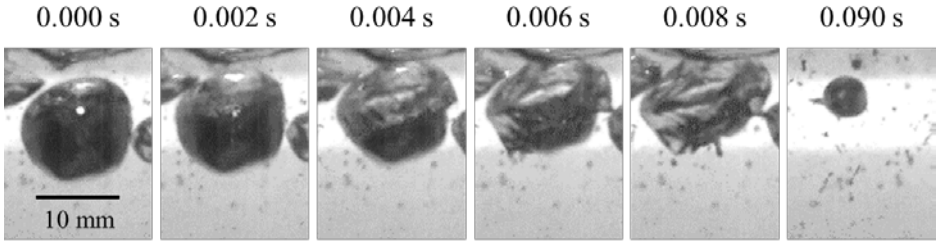

Fig. 5. Snapshots of interface of liquid Sn film. The film ruptured starting at 0.002 s, and a single Ar gas bubble rose in the molten salt and burst at the salt surface. At 0.090 s, the photograph shows a metal drop that was detached from a bubble. In this experiment, the system temperature was 823 K (550 °C), and the flow rate was 8.333 ml/s.

1

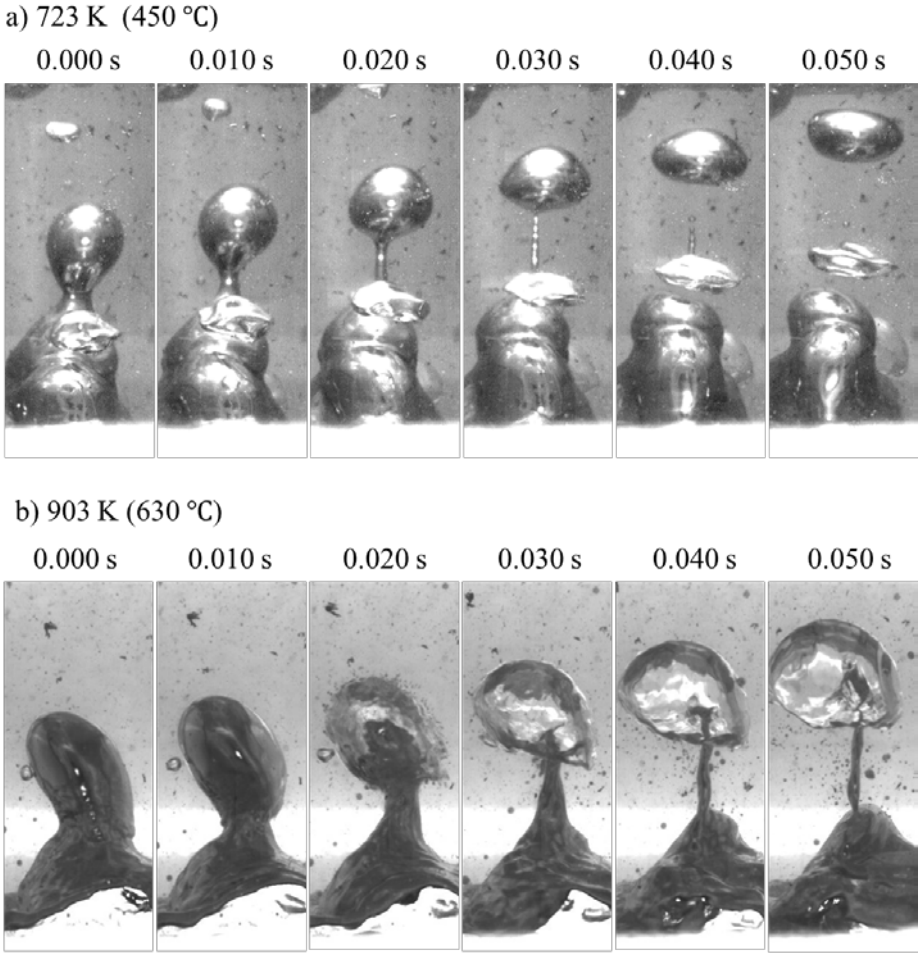

Fig. 6. Comparison of representative experimental photographs of liquid Sn interface behavior at each temperature. Flow rate of Ar gas is controlled at 8.333 ml/s.

SN

1

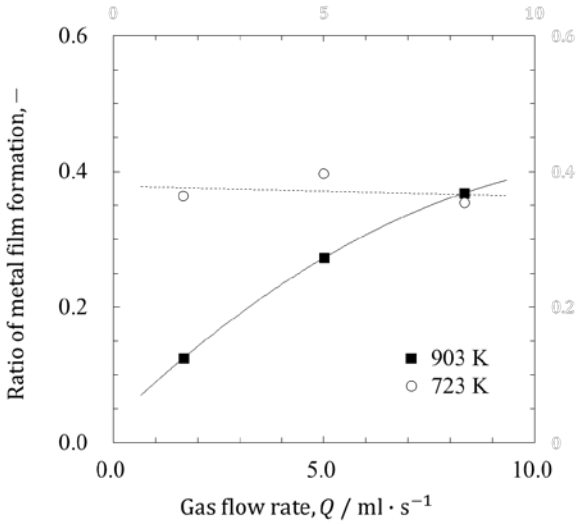

Fig. 7. Gas flow rate dependence of the ratio of metal film formation at each temperature.

1 Table 1 Temperature-dependent equation of physical properties of liquid Sn and molten LiCl–KCl eutectic melt.

ρ_{Sn} [kg/m^3] (Wang and Mei, 2006)	$7406 - 0.994T + 2.12 \times 10^{-4}T^2$
μ_{Sn} [Pa · s] (Rozhitsina, et al. 2011)	$0.31 \times 10^{-3} \exp\left(\frac{6171}{RT}\right)$
σ_{Sn} [N/m] (Yuan et al., 2001)	$0.322 - 3.03 \times 10^{-7}T^2 + 4.32 \times 10^{-3}T$ ($P_{O2} = 8.56 \times 10^{-6}$MPa)
$\rho_{LiCl-KCl}$ [kg/m^3] (Janz et al., 1975)	$2029 - 0.53T$
$\mu_{LiCl-KCl}$ [Pa · s] (Janz et al., 1975)	$8.51 \times 10^{-3} - 7.40 \times 10^{-6}T - 4.86 \times 10^{-9}T^2 + 4.81 \times 10^{-12}T^3$
$\sigma_{LiCl-KCl}$ [N/m] (Janz et al., 1975)	$0.19 - 8.24 \times 10^{-5}T$